PCCP
Physical Chemistry Chemical Physics

Accepted Manuscript

This article can be cited before page numbers have been issued, to do this please use: K. Yamaguchi, K. Kobayashi, K. Ishii, Y. Zhou, Y. Yokoyama, T. Sakka and N. Nishi, *Phys. Chem. Chem. Phys.*, 2026, DOI: 10.1039/D6CP01551D.

ROYAL SOCIETY OF CHEMISTRY

rsc.li/pccp

View Article Online
DOI: 10.1039/D6CP01551D

Three-dimensional electric double layer at solvent-free liquid/liquid interface between two immiscible ionic liquids

Kazuma Yamaguchi[1], Kazuya Kobayashi[1], Kosuke Ishii[2], Yishan Zhou[1], Yuko Yokoyama[1], Tetsuo Sakka[1] and Naoya Nishi[1]

[1]*Graduate School of Engineering, Kyoto University, Kyoto 615-8510, Japan*,

[2]*High Energy Accelerator Research Organization, Ibaraki 319-1106 Japan*

**Corresponding author: Naoya Nishi: nishi.naoya.7e@kyoto-u.ac.jp*

Abstract

The structure of the electric double layer (EDL) at a liquid/liquid interface between hydrophobic and hydrophilic ionic liquids (ILs), trioctylmethylammonium bis(nonafluorobutanesulfonyl)amide (TOMAC4C4N) and ethylammonium nitrate (EAN), was explored using molecular dynamics (MD) simulation. Analyses of the charge density distribution and radial distribution function at this solvent-free IL/IL interface revealed that the smaller ions constituting the hydrophilic EAN phase are inserted into the interfacial "pockets" formed by the capillary wave, whose minimum wavelength is determined by the sizes of the larger ions constituting the hydrophobic TOMAC4C4N phase. The larger ions at the interface were coordinated by the smaller ions across the interface, forming overscreening ionic layers because of the absence of solvents. This specific interfacial ion coordination led to a three-dimensional EDL, in which the smaller counterions in the interfacial "pockets" interact closely with the larger ions. This contrasts with the case at the conventional oil/water interface, where ions in the water phase are hydrated and cannot be inserted into the "pockets", forming a two-dimensional EDL that is insensitive to the interfacial roughness. Simulations of various types of liquid/liquid interfaces found that this unique EDL structure is not specific to the IL/IL interface: the amphiphilicity of smaller ions and the interfacial structure of the larger ions play a key role. Moreover, when a smaller ion in the hydrophilic IL phase is transferred to the hydrophobic IL phase, the ion is often accompanied by other smaller ions, forming an "ionic liquid finger".

Keyword: ITIES, water-free, water finger, ion transfer

View Article Online
DOI: 10.1039/D6CP01551D

1. Introduction

The interface between two immiscible electrolyte solutions (ITIES), so-called the electrochemical liquid/liquid interface, can be electrochemically polarized within the potential window. The edges of the window are defined by the transfer of supporting electrolyte ions dissolved in one liquid phase to the other. Since 1902 when Nernst and Riesenfeld[1] reported that ion transfers can be controlled by applying potential at the phenol/water interface, electrochemical oil (O)/water (W) interfaces have been intensively studied[2-15]. Furthermore, new ITIES systems other than the O/W interfaces have been discovered, such as O/O[16-18], fluorous solvent (F)/W[19-23], ionic liquid (IL)/W[24-32], and IL/O interfaces[33-36].

ILs are salts in the liquid state around room temperature. They are solvent-free and have specific properties such as flame resistance, high ionic conductivity, and high structural designability[37]. Particularly, the high structural designability of cations and anions endows ILs with a wide variety of physicochemical properties. Electrochemistry at the IL/W interface has been enabled by designing IL ions to possess high hydrophobicity[26, 38, 39], and oppositely, at the IL/O interface with IL ions of high hydrophilicity[33-36]. ILs are known to form specific structures in the bulk and at the interface. In the IL bulk, it has been reported from molecular dynamics (MD) simulation that alternating ionic shells are formed around a central ion of interest[40]. At the interface, ILs also form alternating ionic layers, which have been known as overscreening[31, 41-48]. These features are unique to ILs, which are solvent-free, and are not observed in conventional electrolytes.

In this study, by the designability and unique local structures, we focused on the IL-IL two-phase system composed of trioctylmethylammonium bis(nonafluorobutanesulfonyl)amide (TOMAC4C4N) and ethylammonium nitrate (EAN), which were used as the hydrophobic and hydrophilic IL for an electrochemical IL/W[49, 50] and IL/O[33, 36] interface, respectively. The two-phase system of two immiscible ILs has already been reported[51-65], however, the interfacial structure has not yet been explored either with or without potential control. The IL-IL two-phase system has promising applications in hydrocarbon separation[53], metal ion extraction[55, 57, 59, 61], and metal nanoparticle synthesis[60]. In the latter two applications, ion and electron transfer occur across the IL/IL interface, making an understanding of the electric double layer (EDL) structure essential. This system is expected

View Article Online
DOI: 10.1039/D6CP01551D

to be a new class of ITIES, electrochemical IL/IL interface, and furthermore, an IL-specific EDL—unlike that at conventional liquid/liquid interfaces—is expected at the IL/IL interface.

The present study aims to elucidate the microscopic structure and potential dependence of an electrochemical IL/IL interface using a molecular dynamics (MD) simulation, to uncover the physicochemical properties of solvent-free liquid/liquid interfaces. MD simulations are a powerful method to support experimental results and to reveal microscopic structures that are difficult to elucidate experimentally. Three electrochemical liquid/liquid interfaces have been previously investigated using MD simulations, the O/W[66], IL/W[67], and F/W[20] interfaces. The EDL structure at the O/W interface[66] was reported to be the discrete Helmholtz-type, where cations in one liquid phase and anions in the other liquid phase interact closely across the interface. At the IL/W[67] and F/W[20] interfaces, hydrophobic ions in IL or F (IL was added as the supporting electrolyte) formed the interfacial ionic layers without a diffuse layer, whereas ions in W formed a Gouy-Chapman-type EDL. At a solvent-free IL/IL interface, ions are in contact with each other not only within the liquid phases but also across the interface, which would lead to an interfacial structure that differs from the conventional EDL. In this study, we introduce the solvent-free IL/IL interface as a new class of electrochemical liquid/liquid interfaces. Notably, the IL/IL interface forms a specific EDL in which small hydrophilic IL ions are inserted into the interfacial "pockets" created by the interfacial roughness, forming a three-dimensional EDL.

2. MD Simulation

2.1. System

An IL-IL two-phase system was prepared using EAN ($[EA^+]NO_3^-$, Fig. 1a) as the hydrophilic IL phase and TOMAC4C4N ($[TOMA^+][C4C4N^-]$, Fig. 1b) as the hydrophobic IL phase. Two graphene layers (GRs) sandwiching the IL-IL two-phase system were used as electrodes to polarize the IL/IL interface (Fig.2). The force field employed was on the framework of OPLS-AA[68]. The force field parameters were taken from the literature as follows: Jorgensen et al. in 2024[69] for EA^+ and the alkyl chains of $TOMA^+$; CL&P[70] for NO_3^- [71], $C4C4N^-$[72], and around the N atom in $TOMA^+$[73, 74] (see Fig. S1, Table S1-4). For the force field for sp^2 carbons of GR, the bond,

View Article Online
DOI: 10.1039/D6CP01551D

angle, and dihedral potentials were adopted from the OPLS-AA parameters with bond lengths of 1.42 Å and angles of 120°. Since non-polarizable force fields overestimate the electrostatic interactions in ILs, the ionic charges were scaled by a factor of 0.8 to account for the effect of electronic polarization[71, 75]. The compositions in the system were shown in Table S5.

2.2. Simulation details

The equations of motion were calculated by using the leap-frog algorithm. For non-bonded interactions, the Lenard-Jones and the coulombic potentials had a cutoff of 12 Å. The electrostatic calculation was carried out by using the PME method with an accuracy of 1.0×10^{-5}. To constrain the C–H and N–H bond lengths, the LINCS algorithm was used. The simulation time step was 2 fs. The energy minimization of the initial configuration in the system was carried out with the target maximum force of 100 kJ/(mol nm). A v-rescale thermostat[76] (coupling constant: 2.0 ps) and a c-rescale barostat[77] (coupling constant: 4.0 ps) were used to equilibrate the system at 400 K and 1 bar. The bulk simulation for each IL phase was performed under 3-dimensional periodic boundary conditions using the NPT ensemble for 10 ns. The equilibrated bulk structures of the two IL phases were used in the initial configuration for interfacial simulations. A rectangular simulation box (4.673 nm × 4.686 nm × 80.00 nm) was prepared, in which the two IL phases were aligned and sandwiched between two GR sheets along the *z*-axis to form a GR|TOMAC4C4N|EAN|GR configuration, as shown in Fig. 2. The liquid length in the *z*-direction for both IL phases was longer than 10 nm, which is sufficient to prevent overlap of the two electric double layer (EDL) structures within each IL phase (see Section 3.1 for the results). In the *xy*-directions, the cell width (~4.6 nm) was made long enough compared with the minimum wavelength of the capillary waves at the IL/IL interface, which is determined by the size of the large ions, $TOMA^+$ and $C4C4N^-$, ~10 Å.

While fixing the *x* and *y* coordinates of the C atoms of the two GR sheets and applying 1 bar to the sheets from the vacuum sides, the system was equilibrated under the NVT ensemble for 10 ns. After equilibration, the *z* positions of the GR sheets were fixed so that their distance matches the average one (26.88 nm) during the equilibration run. The system was then equilibrated again under the NVT ensemble for 20 ns. This final structure was used as the initial configuration for the uncharged interfacial system. For the charged system, the C atoms of the two GR sheets were

View Article Online
DOI: 10.1039/D6CP01551D

charged evenly with the same magnitude but in the opposite sign; The surface charge of the GR sheet on the EAN side $q_{\mathrm{GR,EAN}}$ was 0.00, ± 3.68, ± 7.32 μC cm^{-2}, with that on the TOMAC4C4N side $q_{\mathrm{GR,TOMAC4C4N}}$ being $-q_{\mathrm{GR,EAN}}$. The system was equilibrated under the NVT ensemble for 20 ns. Both the uncharged and charged systems were analyzed with a 100 ns production run with the Yeh–Berkowitz correction[78]. Five independent simulations with different initial structures were averaged. Trajectories were recorded every 10 ps for atomic coordinates. All simulations were performed using GROMACS 2021.2[79].

2.3. Analysis of trajectory

The MD trajectories were analyzed to obtain the number density distribution along the *z*-axis direction $\rho_i(z)$. The representative points were their N atoms for all the four ions ($TOMA^+$, $C4C4N^-$, EA^+, and NO_3^-; see Fig.1). The charge density distribution $\rho_{\mathrm{c,\,total}}(z)$ was calculated by multiplying $\rho_i(z)$ by the charge of each atom in the force field q_i^{FF} (eq. 1).

$$\rho_{\mathrm{c,\,total}}(z) = \sum_i q_i^{\mathrm{FF}} \rho_i(z) \quad (1)$$

The potential distribution $\phi(z)$ was obtained by numerically integrating the Poisson equation in the *z*-axis twice (eq. 2).

$$\frac{\mathrm{d}^2\phi(z)}{\mathrm{d}z^2} = -\frac{\rho_{\mathrm{c,\,total}}(z)}{\varepsilon_0 \varepsilon_{\mathrm{r}}} \quad (2)$$

where ε_0 was the dielectric constant of the vacuum, and the relative permittivity ε_{r} was set to 1. The potential was referenced to the vacuum phase on the TOMAC4C4N side. The bulk potentials of TOMAC4C4N phase $\phi_{\mathrm{TOMAC4C4N}}$ and EAN phase ϕ_{EAN} were evaluated by averaging the potentials in their bulk *z* region of 10~15 nm and 20~25 nm, respectively. The interfacial potential difference $\Delta\phi$ was defined as their difference ($\phi_{\mathrm{EAN}} - \phi_{\mathrm{TOMAC4C4N}}$).

Two-dimensional mapping of the orientation angle distribution vs. *z*-axis was obtained by mapping the orientation angle distribution $d(z, \theta)$ of an interatomic vector in the *z* region $z \sim z +$ d*z* (d*z* = 0.1 nm). The orientation angular distribution was normalized to satisfy eq. 3.

$$\int_0^{\pi} d(z,\theta) \sin\theta \mathrm{d}\theta = \quad (3)$$

where θ is the angle of the interatomic vector with respect to the *z*-axis (Fig. 3a). The orientation

View Article Online
DOI: 10.1039/D6CP01551D

of the following interatomic vectors were analyzed; for $TOMA^+$, two vectors from the N atom to the terminal C atoms of the methyl and octyl groups; for $C4C4N^-$, vectors from the N atom to the terminal C atoms of the perfluorobutyl groups; for EA^+, a vector from the N atom to the terminal C atom of the ethyl group; for NO_3^-, a vector normal to the plane formed by three O atoms (Fig. 3b).

The three-dimensional radial distribution function $g(r)$ was obtained using eq. 4.

$$g(r) = \frac{n(r)}{4\pi r^2 \mathrm{d}r} \quad (4)$$

where r was the distance of the target atom from the central atom, and $n(r)$ is the number of target atom between $r \sim r + \mathrm{d}r$ ($\mathrm{d}r = 0.01$ nm). $g(r)$ was normalized to converge to 1 in the bulk.

3. Results and discussion

3.1. Interfacial potential difference

Charging the two GR electrodes with an equal magnitude and opposite sign imposed a potential difference across the IL-IL two-phase system. Fig. 4 shows the potential profiles along the z-axis. In each bulk region (TOMAC4C4N phase; 3 nm < z < 11 nm, EAN phase; 15 nm < z < 22 nm), the potentials were flat, and the potential shifts were observed only at the GR/TOMAC4C4N, TOMAC4C4N/EAN, and EAN/GR interfaces. These shifts indicated that the interfacial charges were sufficiently screened, resulting in the formation of EDLs at these three interfaces. The EDLs at the two IL/GR interfaces showed alternately charged ionic multilayers, like those observed in our previous MD studies[20, 31, 67, 80, 81]. The potential profiles in the vicinity of the TOMAC4C4N/EAN interface (z = ~12.5 nm), which is the new electrochemical liquid/liquid interface investigated in the present study, are shown in Fig. 4b. The interfacial potential difference at the TOMAC4C4N/EAN interface was 0.00 V at $q_{\mathrm{GR,EAN}}$ = 0.00 μC cm^{-2} and increased to +0.08 and –0.13 V upon charging up the GRs with $q_{\mathrm{GR,EAN}}$ = +7.32 and –7.32 μC cm^{-2}, respectively, demonstrating that the IL/IL interface is polarizable. At $q_{\mathrm{GR,EAN}} = \pm 7.32$ μC cm^{-2}, we observed a rare event where an ion in the EAN phase transferred to the TOMAC4C4N phase, indicating that the potential is at the potential window edge at these charging conditions and that the potential

View Article Online
DOI: 10.1039/D6CP04551D

window width is 0.2 V. This potential window coincides with the experimental one (Fig. S2, 3) obtained with electrochemical measurements at liquid/liquid interfaces formed at a micropipette-tip[26, 27, 36]. Assuming a linear relationship between the surface charge density $q_{\mathrm{LL,EAN}}$ on the EAN side of the IL/IL interface and the interfacial potential difference $\Delta\phi$, the capacitance ($q_{\mathrm{LL,EAN}}/\Delta\phi$) was estimated to be 64 μF cm^{-2} (Fig. S4). This value is significantly larger than those reported for other electrochemical liquid/liquid interfaces, 10 times higher than that of the O/W interface[66] and three times higher than that of the IL/W interface[67].

To identify the origin of this unusually high capacitance, the total charge density distribution, $\rho_{\mathrm{c,total}}(\mathrm{z})$, at the IL/IL interface was examined (Fig. 5a). In the bulk of each phase (z < 11 nm, z > 15 nm), the charge density was zero, however, at the interface, slight deviations from zero in the form of small peak pairs were observed. These peak magnitudes are significantly smaller than those reported previously for the O/W[66] and IL/W[67] interfaces, where distinct positive and negative peaks were spatially separated along the z-axis, consistent with a Helmholtz-type or Gouy-Chapman-type EDL. To investigate this unusual polarizability behavior, the total charge density distribution was decomposed into the two contributions from the TOMAC4C4N ($TOMA^+$, $C4C4N^-$) and EAN (EA^+, NO_3^-) phases (Fig. 5b). When the GRs were negatively (positively) charged, positive (negative) peaks appeared on the TOMAC4C4N side of the interface, while negative (positive) peaks appeared on the EAN side. This switching was caused by ion accumulation at the interface such as a cation (anion)-rich on the TOMAC4C4N side and an anion (cation)-rich on the EAN side (Fig. S5), which has already been reported for the electrochemical liquid/liquid interfaces[20, 66, 67]. Notably, the charged EDL regions of the two phases overlapped in the z-axis. This overlap led to the cancellation of positive and negative charge peaks within the xy plane, resulting in a reduction in the total charge density. The surface charge density of the accumulated ions on the TOMAC4C4N and EAN sides of the interface is equal in magnitude to q_{GR} (Fig. S6); therefore, this apparent enhancement of the capacitance arises from an underestimation of the interfacial potential difference. This behavior is different from the EDL structures of conventional electrochemical liquid/liquid interfaces[20, 66, 67], where the overlap of the positive and negative peaks was marginal. This peak overlap can be attributed to either an interfacial mixed layer[82, 83] of ILs or the interdigitation of two immiscible ILs at the interfacial

View Article Online
DOI: 10.1039/D6CP01551D

region.

3.2. Interfacial "pockets" and insertion of ions

To examine the ionic behavior at the IL/IL interface, the in-plane distribution of ions at the interface was analyzed using MD snapshots. Fig. 6a shows how to view the IL/IL interface from the EAN phase side. On the TOMAC4C4N side (Fig. 6b-d), all atoms consisting the IL were displayed, while on the EAN side (Fig. 6e-g), only EAN atoms with $z < (Z_{min} + Z_{max})/2$ were shown, where Z_{min} and Z_{max} are the minimum z-coordinate of the atoms in the EAN phase and maximum z-coordinate of the atoms in the TOMAC4C4N phase, respectively (see Fig.6a). In Fig. 6c, on the TOMAC4C4N side at electrical neutrality ($q_{GR,EAN}$ = 0.00 μC cm^{-2}), the N atoms of $TOMA^+$ (green) and $C4C4N^-$ (purple) were evenly distributed at the interface. With the charge applied to the interface ($q_{GR,EAN}$ = ± 7.32 μC cm^{-2}, Fig. 6b, d), the EDL switched to either a cation-rich or anion-rich state, consistent with the density profiles in Figs. 5b and S5b. In Fig. 6f, on the EAN side at $q_{GR,EAN}$ = 0.00 μC cm^{-2}, multiple EA^+ (red) and NO_3^- (blue) were unevenly distributed in the area occupied by hydrophobic ions. At $q_{GR,EAN}$ = ± 7.32 μC cm^{-2} (Fig. 6e, g), similar aggregates were observed. Considering the difference in ionic radius between the two phases (Fig. S7), these hydrophilic ion aggregates suggested the formation of interfacial "pockets" due to the interfacial roughness rather than a mixed IL layer. Here, the size of the "pockets" was comparable to the minimum wavelength of the capillary waves at the IL/IL interface, which was determined by size of large ions, $TOMA^+$ and $C4C4N^-$, ~10 Å.

We hypothesized that the ionic aggregation in the "pockets" is due to the absence of solvent molecules, since solvation would inherently prevent the aggregation. To confirm the validity of this hypothesis, we investigated the TOMAC4C4N/W(EAN) interface, diluting the EAN phase with water. Fig. 7 shows the snapshots of the interface at $q_{GR,EAN}$ = +7.32 μC cm^{-2}, where cations were accumulated on the EAN side and anions on the TOMAC4C4N side, viewed in the same way as Fig. 6e. At the IL/IL interface (Fig. 7a), one can see the aggregates of smaller ions, EA^+ (red) and NO_3^- (blue), partly inserted into the interface "pockets". In contrast, at the TOMAC4C4N/W(EAN) interface (Fig. 7b), the ion aggregates were not observed, and the number of the inserted ions drastically decreased. To further confirm this hydration effect, we replaced EA^+

View Article Online
DOI: 10.1039/D6CP01551D

with Li^+, a hard ion with a strong hydration shell. In Fig. 7c for the TOMAC4C4N/W($LiNO_3$) interface, the ion insertion into the interfacial "pockets" was strongly suppressed. The snapshots for the three liquid/liquid interfaces shown in Fig.7 illustrate that significant ion insertion occurred only at the solvent-free IL/IL interface. Notably, for the two IL/W interfaces, the total charge density distribution, $\rho_{c,total}(z)$, exhibited clear positive and negative peaks (Fig. S8), consistent with the previous studies[20, 66, 67] although they were partly overlapped along the z-axis. We note here that the interfacial roughness, the total amplitude of the capillary waves, at the IL/IL interface was 2.5 Å, comparable to that of the IL/W interfaces (Fig. S9). The interfacial roughness did not significantly change regardless of the applied potential. We also note that these are smaller than experimentally obtained values at O/W interfaces[8], because of the underestimation in MD caused by cell size limitations. Considering the minimum wavelength of the capillary wave is determined by the size of the larger ions, the size (depth and width) of the interfacial "pockets" at these three interfaces is also comparable. In other words, the differences in the EDL structures between the IL/IL and IL/W interface are induced by water, which plays a crucial role in determining the EDL structure at liquid/liquid interfaces.

To further illuminate how water molecules disrupt ion aggregation at the interface, the distribution of ion aggregations between $TOMA^+$ and NO_3^- was investigated. Fig. 8 shows the number density distribution, at $q_{GR,EAN}$ = 0.00 μC cm^{-2}, of the N atom of $TOMA^+$ classified by the coordination number of NO_3^- within a cutoff distance of 0.67 nm which corresponds to the first coordination shell of the N atom of NO_3^- around the N atom of $TOMA^+$ (Fig. S10). Fig. 8a shows that, in the TOMAC4C4N bulk (z < 10 nm), the number densities of N atoms not coordinated by NO_3^- are equal to the total number of N atoms because no NO_3^- exists in this phase. At the IL/IL interface (10 nm < z < 14 nm, Fig.8b), $TOMA^+$ was coordinated by NO_3^- in the EAN phase across the interface, and the coordination number increased up to 5 as the $TOMA^+$ position is closer to the interface. On the other hand, at the IL/W interfaces, $TOMA^+$ was coordinated with no more than two NO_3^- (Fig. 8c, e) and remained predominantly surrounded by more than 5 water molecules across the interface (Fig. 8d, f). Because of the capillary wave on the IL/IL interface, $TOMA^+$ at the IL/IL interface are protruded to or receded from the EAN side. The receded $TOMA^+$ at the IL/IL interface could be coordinated by only a few NO_3^-, whereas for the protruded $TOMA^+$

View Article Online
DOI: 10.1039/D6CP01551D

the coordination number of NO_3^- increased. These interfacial structures allowed ions in the TOMAC4C4N phase to be coordinated with the hydrophilic ions in the EAN phase across the interface, similarly to interfacial ion pairing at the interface previously discussed[84-87]. In contrast, hydrated NO_3^- at IL/W interfaces, whose roughness was comparable to the IL/IL interface, were excluded from the interfacial "pockets". Thus, ion insertion is governed by two factors: the size difference between the hydrophobic and hydrophilic ions and the presence of solvents. For the former, the larger the large ions are compared with the small ions, the more room the interfacial "pockets" provides for the small ions. For the latter, solvation makes it difficult for the solvated and enlarged small ions to enter the "pockets". In the solvent-free system studied here, these two requirements are satisfied, leading to the formation of the specific EDL structure, whereas in the conventional liquid/liquid interfaces[20, 66, 67], the EDL structure has been reported under conditions where a solvent (water) is present and hard ions are employed as supporting electrolytes in the hydrophilic phase. As shown in Fig. 9a, the EDL structure at the conventional liquid/liquid interfaces[20, 66, 67] is more like two-dimensional, in which cations and anions indirectly interact face-to-face across the interface due to the solvent presence. On the other hand, at the IL/IL interface (Fig.9b), cations and anions interact with ion coordination across the interface, where the EDL is formed along the capillary wave-roughened interface and is more like three-dimensional.

3.3. Ionic structure at the interface

3.3.1. Interaction between hydrophilic IL and hydrophobic IL

To elucidate the microscopic interfacial structure and local ionic environments at the IL/IL interface, radial distribution functions (RDFs) and coordination numbers were analyzed. Fig. 10 shows the atom–atom RDFs around the N atom of $TOMA^+$ at $q_{GR,EAN}$ = 0.00 μC cm^{-2} in the interfacial region (see S10, Fig.S11, and Table S6 for the definition). Fig. 10a shows that at the TOMAC4C4N/EAN interface, the N atom of $TOMA^+$ exhibited a first coordination peak with the N atom of NO_3^-, reflecting the ion coordination across the interface, while $TOMA^+$–EA^+ correlations appeared from the second coordination shell. These RDFs exhibited an oscillatory distribution of the cation and anion in an out-of-phase manner, which eventually converged in the bulk region. This oscillatory distribution was typically shown in the bulk of ILs[40] and even at the

View Article Online
DOI: 10.1039/D6CP01551D

interface of ILs as oversceening[31, 41-43]. The same analysis at the IL/W interfaces (Fig. 10b, c) shows that the $TOMA^+$–NO_3^- coordination in the first shell persisted, while the second cationic peaks (EA^+ or Li^+) were markedly suppressed, indicating that water destroyed the overscreening structure. At the TOMAC4C4N/W (EAN) interface (Fig. 10b), the EA^+ distribution exhibited a weak coordination peak at 0.7 nm, whereas at the TOMAC4C4N/W ($LiNO_3$) interface (Fig. 10c), no Li^+ peak appeared. This difference between EA^+ and Li^+ could be attributed to the amphiphilicity of EA^+, which, owing to its non-polar ethyl group, could approach the hydrophobic IL phase more closely than hydrated Li^+.

Fig. 11 shows the potential dependence of the RDFs and coordination numbers of EA^+ and NO_3^- around the N atom of $TOMA^+$ in the first coordination shell of NO_3^- at the TOMAC4C4N /EAN interface. Fig. 11a shows the structure in which cations and anions in the EAN phase are alternately coordinated with $TOMA^+$, as described above (Fig.10a). At $q_{GR,EAN} < 0$ μC cm^{-2}, where $TOMA^+$ and NO_3^- were enriched at the interface, the first peak in the RDF between $TOMA^+$ and NO_3^- increased in intensity, but the position remained unchanged. The first coordination peak of EA^+ similarly increased in intensity and slightly shifted closer to $TOMA^+$. The increased intensity of the first peaks in the two RDFs suggests an increased number of both cations and anions in the first coordination shell, as observed in the EDL overscreening behavior in ILs at flat electrodes. For the coordination number (Fig.11b), at $q_{GR,EAN} = 0.00$ μC cm^{-2}, $TOMA^+$ was coordinated by three NO_3^- and two EA^+, resulting in local charge neutrality at the interface. When $TOMA^+$ and NO_3^- were enriched at the interface ($q_{GR,EAN} < 0$ μC cm^{-2}), the coordination number increased for not only NO_3^- but also EA^+, which again follows the overscreening behavior. Specifically, NO_3^- accumulated in the first coordination shell of $TOMA^+$ to compensate for its charge; however, in the absence of solvent, small ions such as EA^+ contributed to the excess charge compensation of NO_3^-, leading to the formation of local overscreening, analogous to that observed in the bulk [38] and at the interface[31, 41-43] of ILs. Accordingly, the shift of the first peak in the RDF of EA^+ shown in Fig. 11a results from the increased population of overscreening NO_3^- at $q_{GR,EAN} < 0$ μC cm^{-2}, which enhanced the attraction of EA^+ in the second coordination shell. Consequently, at the solvent-free IL/IL interface, locally alternating layers of cations and anions are formed, which leads to a three-dimensional EDL (Fig. 9b). On the other hand, at the IL/W interface, the

View Article Online
DOI: 10.1039/D6CP01551D

hydration of ions in the W phase suppresses ion coordination across the interface, rather, interfacial ionic interactions are predominantly water-mediated, which suggests a two-dimensional EDL (Fig.9a).

Based on the discussion so far, the following considerations can be made regarding the EDL structure at the liquid/liquid interface between water and a hydrophobic liquid. When the W phase contains ions that are easily hydrated (ex. Li^+, EA^+, Cl^-, NO_3^-) as the supporting electrolyte, a two-dimensional EDL is formed because of the solvation of the ions. However, as shown in Fig. S12a, when the W phase contains amphiphilic ions that are not easily hydrated but are smaller than the size of the interfacial "pockets", such as tetramethylammonium (TMA^+) in Fig.S12a, the ions are inserted into the "pockets". For this case, whether the EDL is two-dimensional or three-dimensional depends on the interfacial structure on the hydrophobic side. If large ions whose polar groups are surrounded by bulky nonpolar groups (ex. bis-triphenyl phosphoranylidene ammonium[66], tetrakispentafluorophenylborate[66], and tetrakis[3,5-bis(trifluoromethyl)phenyl] borate[26]) are chosen as the supporting electrolyte in the hydrophobic phase or constitute the phase itself as an IL, the polar groups of the large ions cannot be protruded toward the hydrophilic side of the interface, making it difficult to form a three-dimensional EDL. In contrast, for asymmetric ions with exposed polar and charged groups like $TOMA^+$ and $C4C4N^-$ (Fig.1) in the present study, or ions with flexible side chains like trihexyltetradecylphosphonium ($THTDP^+$)[20, 21, 23], the charge protrusion at the interface facilitates the formation of a three-dimensional EDL (Fig. S12b, c). In other words, the formation of a three-dimensional EDL is determined by (i) how readily ions from both phases can expose their polar groups toward the opposite side of the interface and (ii) how smaller ions can be inserted into the interfacial "pockets", whose size is determined by the capillary wave.

3.3.2. Orientational correlation dependence on the z direction

Fig. 12 shows the two-dimensional mapping of the orientational angle distribution along the z-axis at $q_{GR,EAN} =$ 0.00 μC cm^{-2}. In the color scale of $d(z,\theta)$, light blue, $d(z,\theta) = 1$, represents isotropic orientation, whereas red, higher $d(z,\theta)$ at 3, indicates a polar orientation at a given z-region. The orientation of interatomic vectors was defined as shown in Fig. 3. In the EAN phase in the bulk (z > 13 nm), both the normal vector of three O atoms plane in NO_3^- (Fig. 12a) and the

View Article Online
DOI: 10.1039/D6CP01551D

N–C vector of EA^+ (Fig. 12b) exhibited isotropic distributions. In contrast, within the interfacial region (z < 13 nm), for NO_3^-, at z =12.5 nm, a distribution of the surface normal vector appears around 0 and 180 degrees, indicating that NO_3^- plane was oriented along the interface. This orientation implies in-plane electrostatic interactions between the negatively charged O atoms of NO_3^- and the N^+ moiety of the polar-oriented EA^+. The ethyl chain of EA^+ at the interface was preferentially oriented toward the TOMAC4C4N phase. This orientation was energetically favorable because the hydrophobic ethyl group favors the hydrophobic phase over the hydrophilic N^+ moiety. In the TOMAC4C4N phase, the distribution of the octyl chains of $TOMA^+$ varied with z-position. At z = ~12 nm, a distribution appears around 120 degrees, whereas at z = ~13 nm, the distribution becomes concentrated near 135 degrees, loosely pointing to the TOMAC4C4N bulk, similar to the orientation of $C4C4N^-$, vectors from the N atom to the terminal C atoms of the perfluorobutyl groups (Fig. S13). These tendencies were also observed at the IL/W[67] and F/W[20] interfaces. In Fig. 12d, the methyl groups of $TOMA^+$ preferentially oriented toward the EAN phase at z = ~ 13 nm (Fig. 12c), again the same as the previous studies[20, 67]. The z-region of preferential orientation of $TOMA^+$ corresponds to that in which EA^+ and NO_3^- in the EAN phase showed polar ordering (Fig. 12a). These polar ordering of the moiety in $TOMA^+$ indicated that at z = ~13 nm, the protrusion of $TOMA^+$ toward the EAN phase resulted in the bulky octyl chains preferentially oppositely orienting toward the hydrophobic bulk and the methyl chain orienting toward the hydrophilic phase. Moreover, this z-region corresponds to the interfacial region in the charge density distribution (Fig. 5b), suggesting that the specific EDL structure is governed by interactions between polar-oriented ions.

4. The formation of "IL finger"

At $q_{GR,EAN}$ = +7.32 μC cm^{-2}, we observed a phenomenon where an EA^+ ion is transferred from the EAN into TOMAC4C4N phase, although it happened infrequently. This indicates that the interfacial potential at this charged state is at the edge of the potential window. This is also the case with NO_3^- transfer to the TOMAC4C4N phase at $q_{GR,EAN}$ = –7.32 μC cm^{-2}. When ions in the EAN phase are about to transfer to the TOMAC4C4N phase, a structure was formed where the transferring ion is accompanied by other ions in the EAN phase. We call this structure "ionic liquid

View Article Online
DOI: 10.1039/D6CP01551D

finger", shown in Fig. 13. This term comes from "water finger" at the O/W interfaces, which is formed during the transfer of a hydrophilic ion from W to O[7], thereby lowering the intermediate Gibbs energy during the transfer[88, 89]. As Marcus previously proposed,[88] during the ion transfer across a liquid/liquid interface between liquids A and B, the protrusion of liquid A into liquid B and vice versa play important roles in the desolvation/solvation processes for the transferring ions. In the case of the IL/IL interface, when EAN ions transfer into the TOMAC4C4N phase, it is unnecessary for TOMAC4C4N to protrude into the EAN phase because the EAN ions at the IL/IL interface have already completed the first stage of the transfer process, partly desolvated from EAN and partly solvated by TOMAC4C4N. Under these circumstances, two possible transfer mechanisms for a hydrophilic ion are considered: (i) transfer accompanied by the finger structure and (ii) transfer of a sole ion without the finger formation. In mechanism (i), coulombic interactions between unlike ions in the finger reduce the intermediate Gibbs energy, thereby facilitating ion transfer. In mechanism (ii), the large ions in the hydrophobic phase, $TOMA^+$ and $C4C4N^-$, act as a "catalyst" [90], which interact with the transferring small ions across the interface, leading to the ion transfer to the TOMAC4C4N phase without the finger formation.

5. Conclusion

We investigated the EDL structure at the solvent-free IL/IL interface using MD simulation. Amphiphilic ions in the EAN phase were inserted into the "pockets" formed by the interfacial roughness. The large ions in the TOMAC4C4N phase at the interface were coordinated with small ions across the interface, resulting in a three-dimensional EDL. This three-dimensional nature in EDL is not from an increase in the interfacial roughness, but from a solvent-free environment. This was confirmed by the comparison with the IL/W interfaces where the hydrophilic IL is diluted with water, the small ions were hydrated and enlarged, which hindered ionic insertion and interfacial ion coordination, promoting the formation of a two-dimensional EDL. The three-dimensional EDL showed anomalous capacitance enhancement in MD due to charge peak cancellation. However, as predicted in a previous theoretical study on the capacitance at liquid/liquid interfaces,[7] the three-dimensional EDL may, in reality, exhibit a higher capacitance than its two-dimensional counterpart. This will be verified by electrochemical measurements at the IL/IL interface in the future. By

View Article Online
DOI: 10.1039/D6CP01551D

analyzing the EDL structure at the various liquid/liquid interfaces, the EDL structure is determined by two factors: (i) larger ions exposing their polar groups and (ii) small ions inserted into the interfacial "pockets". Moreover, ions in the EAN phase transfer to the TOMAC4C4N phase with an "IL finger" composed of EAN ions.

Author contributions

KY: Investigation, Formal analysis, Writing – original draft, KK: Writing – review & editing, KI: Writing – review & editing, YZ: Investigation, YY ; Writing – review & editing, TS: Writing – review & editing, NN: Project administration, Conceptualization,

Conflict of interest

There are no conflicts to declare.

Acknowledgement

This work was partly supported by the Japan Society for the Promotion of Science (JSPS) KAKENHI Grants (23H03829, 25K01875).

Reference

[1] W. Nernst and E. H. Riesenfeld, Ann. Phys., 313, 600 (1902).

[2] J. Koryta et al., J. Electroanal. Chem., 67, 263 (1976).

[3] C. Gavach et al., J. Electroanal. Chem., 83, 225 (1977).

[4] Z. Samec, Chem. Rev., 88, 617 (1988).

[5] M. Senda et al., Electrochim. Acta, 36, 253 (1991).

[6] I. Benjamin, Science, 261, 1558 (1993).

[7] L. I. Daikhin et al., Electrochim. Acta, 45, 685 (1999).

[8] M. L. Schlossman et al., High Perform. Polym., 12, 551 (2000).

[9] G. Luo et al., Science, 311, 216 (2006).

[10] H. H. Girault, "Electrochemistry at Liquid/Liquid Interfaces" in Electroanalytical Chemistry, ed. A. J. Bard, C. G. Zoski, Vol. 23, CRC Press (2010).

View Article Online
DOI: 10.1039/D6CP01551D

[11] H. H. Girault, Electroanal. Chem., 23, 1 (2010).

[12] Z. Samec, Electrochim. Acta, 84, 21 (2012).

[13] S. G. Booth et al., J. Phys. Chem. C, 119, 23295 (2015).

[14] A. Gamero-Quijano et al., Curr. Opin. Electrochem., 38, 101212 (2023).

[15] J. A. Ribeiro et al., Talanta, 280, 126729 (2024).

[16] M. Suzuki, J. Electroanal. Chem., 372, 39 (1994).

[17] M. Suzuki, J. Electroanal. Chem., 384, 77 (1995).

[18] K. K. Saravanan and R. A. W. Dryfe, Electrochim. Acta, 147861 (2025).

[19] H. Katano et al., J. Electroanal. Chem., 788, 232 (2017).

[20] K. Ishii et al., J. Phys. Chem. C, 129, 16235 (2025).

[21] K. Ishii et al., Electrochim. Acta, 513, 145563 (2025).

[22] K. Uematsu et al., Anal. Sci., 41, 1335 (2025).

[23] K. Ishii et al., Langmuir, 41, 17973 (2025).

[24] B. M. Quinn et al., Langmuir, 18, 1734 (2002).

[25] T. Kakiuchi et al., Electrochem. Commun., 5, 159 (2003).

[26] N. Nishi et al., Anal. Chem., 78, 2726 (2006).

[27] N. Nishi et al., Anal. Chem., 78, 5805 (2006).

[28] J. Langmaier and Z. Samec, Electrochem. Commun., 9, 2633 (2007).

[29] D. S. Silvester and D. W. M. Arrigan, Electrochem. Commun., 13, 477 (2011).

[30] N. Nishi et al., Chem. Commun., 51, 13638 (2015).

[31] S. Katakura et al., J. Phys. Chem. B, 124, 6412 (2020).

[32] L. Nazari and T. J. Stockmann, Langmuir, 40, 24494 (2024).

[33] N. E. A. Cousens and A. R. Kucernak, Electrochem. Commun., 31, 63 (2013).

[34] Y. Kuroyama et al., J. Electroanal. Chem., 881, 114959 (2021).

[35] N. Yoshida et al., Electrochem. Commun., 156, 107575 (2023).

[36] K. Miyazato et al., J. Electroanal. Chem., 954, 118038 (2024).

[37] K. R. Seddon, J. Chem. Technol. Biotechnol., 68, 351 (1997).

[38] T. Kakiuchi and N. Nishi, Electrochemistry, 74, 942 (2006).

[39] R. Ishimatsu et al., Chem. Lett., 36, 1166 (2007).

View Article Online
DOI: 10.1039/D6CP01551D

[40] S. M. Urahata and M. C. C. Ribeiro, J. Chem. Phys., 120, 1855 (2004).

[41] A. A. Kornyshev, J. Phys. Chem. B, 111, 5545 (2007).

[42] M. Mezger et al., Science, 322, 424 (2008).

[43] M. Z. Bazant et al., Phys. Rev. Lett., 106, 046102 (2011).

[44] M. V. Fedorov and A. A. Kornyshev, Chem. Rev., 114, 2978 (2014).

[45] J. P. de Souza and M. Z. Bazant, J. Phys. Chem. C, 124, 11414 (2020).

[46] S. Katakura et al., Phys. Chem. Chem. Phys., 22, 5198 (2020).

[47] N. Nishi et al., Bull. Chem. Soc. Jpn., 94, 2914 (2021).

[48] B. L. Nguyen et al., J. Phys. Chem. Lett., 17, 2374 (2026).

[49] Y. Yasui et al., J. Phys. Chem. B, 113, 3273 (2009).

[50] T. Kakiuchi et al., ChemPhysChem, 11, 2912 (2010).

[51] A. Arce et al., Chem. Commun., 24, 2548 (2006).

[52] S. Cheng et al., Chem. Commun., 24, 2497 (2007).

[53] A. Arce et al., Phys. Chem. Chem. Phys., 10, 2538 (2008).

[54] G. Annat et al., J. Phys. Chem. B, 116, 8251 (2012).

[55] S. Wellens et al., Phys. Chem. Chem. Phys., 15, 9663 (2013).

[56] S. Omar et al., J. Phys. Chem. B, 118, 2442 (2014).

[57] A. Rout et al., RSC Adv., 4, 5753 (2014).

[58] C. M. S. S. Neves et al., J. Phys. Chem. Lett., 8, 3015 (2017).

[59] D. Azizi and F. Larachi, Sep. Purif. Technol., 191, 340 (2018).

[60] Y. Pei et al., Chem. Commun., 54, 6260 (2018).

[61] K. Damarla et al., Langmuir, 34, 10081 (2018).

[62] T. Shimomura and M. Sugiyama, J. Chem. Eng. Data, 63, 402 (2018).

[63] M. A. Rocha et al., J. Chem. Phys., 149, 164502 (2018).

[64] Y. Pei et al., J. Mol. Liq., 366, 120256 (2022).

[65] T. Shimomura et al., J. Chem. Eng. Data, 70, 4689 (2025).

[66] G. C. Gschwend et al., Chem. Sci., 11, 10807 (2020).

[67] K. Ishii et al., Phys. Chem. Chem. Phys., 23, 22367 (2021).

[68] R. C. Rizzo and W. L. Jorgensen, J. Am. Chem. Soc., 121, 4827 (1999).

View Article Online
DOI: 10.1039/D6CP01551D

[69] W. L. Jorgensen et al., J. Phys. Chem. B, 128, 250 (2024).

[70] J. N. Canongia Lopes and A. A. H. Pádua, Theor. Chem. Acc., 131, 1129 (2012).

[71] B. Doherty et al., J. Chem. Theory Comput., 13, 6131 (2017).

[72] A. S. L. Gouveia et al., Phys. Chem. Chem. Phys., 19, 29617 (2017).

[73] J. N. Canongia Lopes and A. A. H. Pádua, J. Phys. Chem. B, 108, 16893 (2004).

[74] J. N. Canongia Lopes and A. A. H. Pádua, J. Phys. Chem. B, 110, 19586 (2006).

[75] A. Mondal and S. Balasubramanian, J. Phys. Chem. B, 118, 3409 (2014).

[76] G. Bussi et al., J. Chem. Phys., 126, 014101 (2007).

[77] M. Bernetti and G. Bussi, J. Chem. Phys., 153, 114107 (2020).

[78] I. Yeh and M. L. Berkowitz, J. Chem. Phys., 111, 3155 (1999).

[79] M. J. Abraham et al., SoftwareX, 1–2, 19 (2015).

[80] S. Katakura et al., J. Phys. Chem. C, 124, 7873 (2020).

[81] S. Zhang et al., Phys. Chem. Chem. Phys., 23, 13905 (2021).

[82] H. H. J. Girault and D. J. Schiffrin, J. Electroanal. Chem., 244, 15 (1988).

[83] W. Schmickler, J. Electroanal. Chem., 428, 123 (1997).

[84] Y. Cheng et al., J. Chem. Soc., Faraday Trans., 87, 107 (1991).

[85] C. M. Pereira et al., J. Electroanal. Chem., 436, 9 (1997).

[86] T. Huber et al., J. Electroanal. Chem., 467, 203 (1999).

[87] R. Ishimatsu et al., Langmuir, 23, 7608 (2007).

[88] R. A. Marcus, J. Chem. Phys., 113, 1618 (2000).

[89] N. Kikkawa et al., J. Am. Chem. Soc., 137, 8022 (2015).

[90] T. Hirano and A. Morita, J. Phys. Chem. B, 124, 3811 (2020).

View Article Online
DOI: 10.1039/D6CP01551D

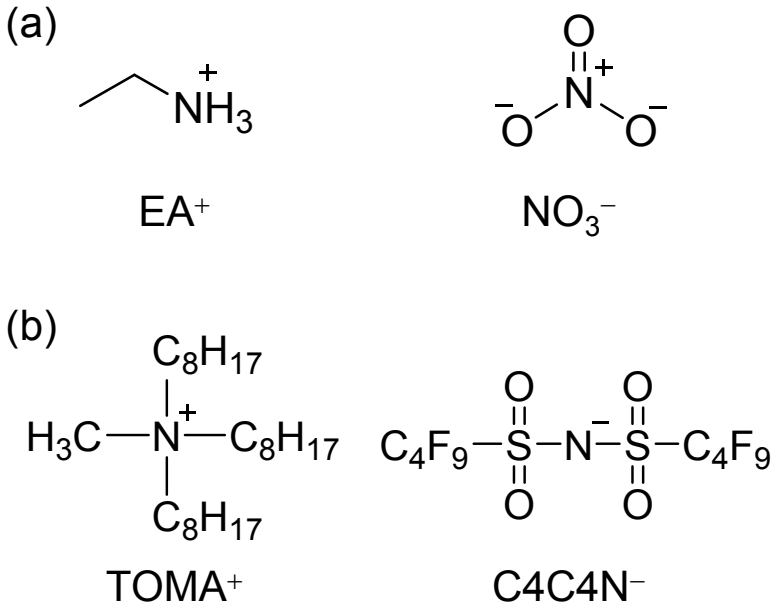

Fig. 1 Ionic structures for the (a) hydrophilic and (b) hydrophobic ILs.

View Article Online
DOI: 10.1039/D6CP01551D

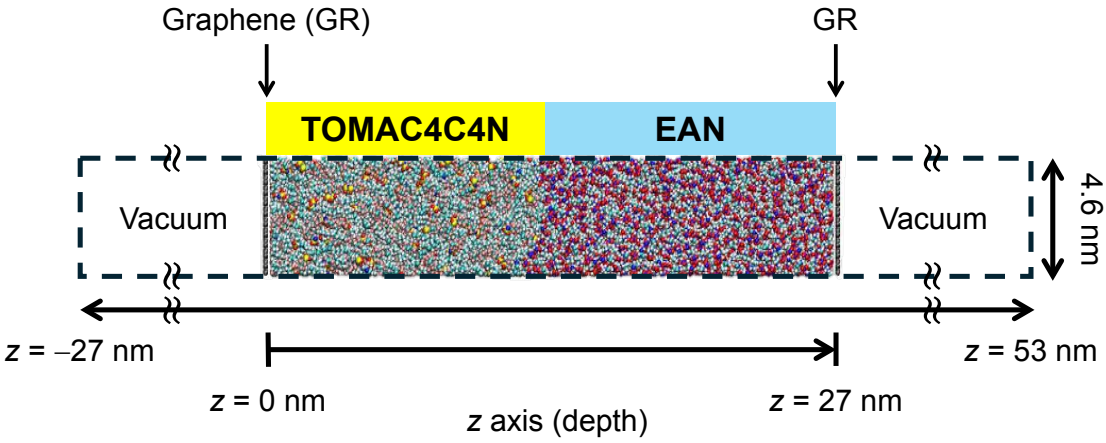

Fig. 2 Simulation box for the IL-IL two-phase system sandwiched with two GR sheets.

View Article Online
DOI: 10.1039/D6CP01551D

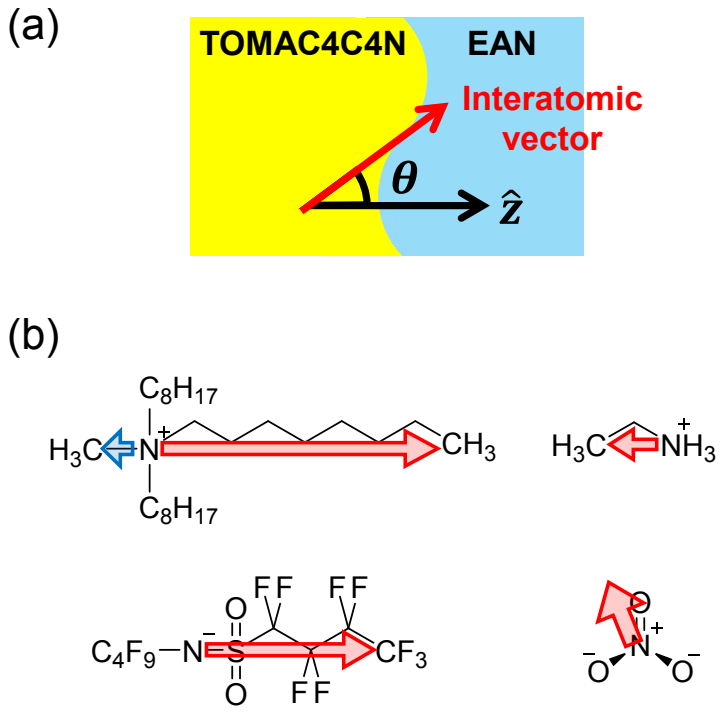

Fig. 3 Definition of (a) the orientation angle θ of an interatomic vector with respect to the *z*-axis and (b) interatomic vectors in ions; for NO_3^-, a vector normal to the plane formed by three O atoms.

View Article Online
DOI: 10.1039/D6CP01551D

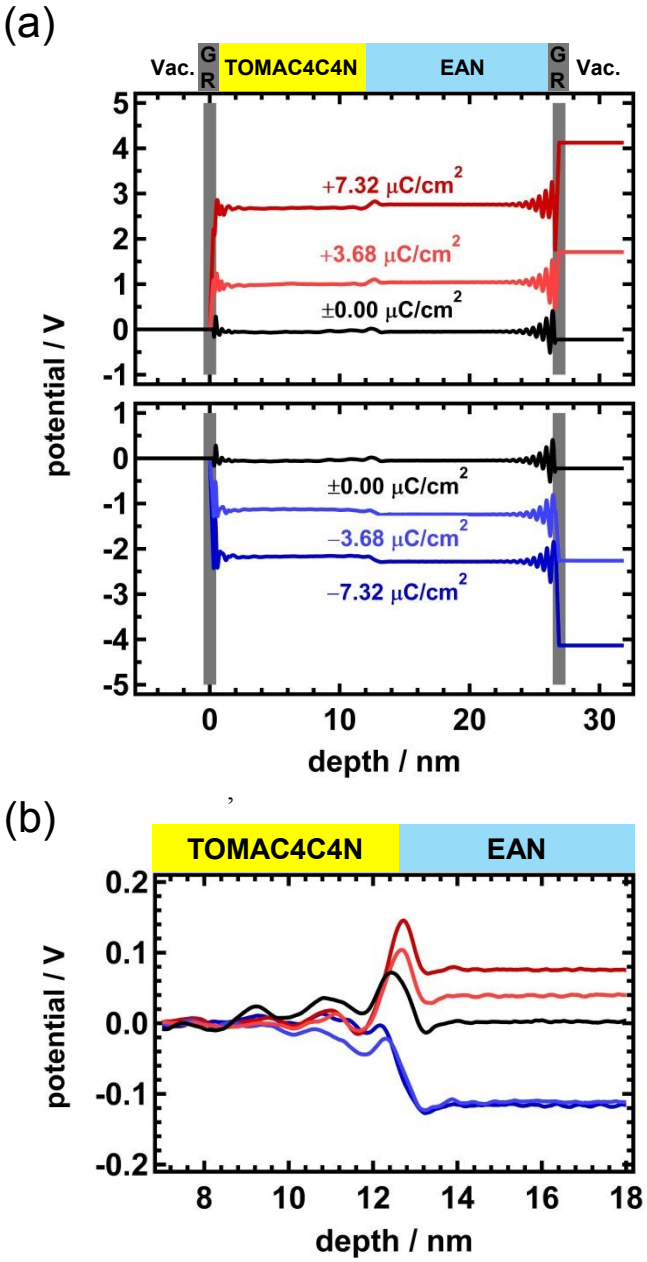

Fig. 4 Potential profiles along the z-axis at various $q_{\mathrm{GR,EAN}}$ values; +7.32 (dark red), +3.68 (red), 0.00 (black), −3.68 (light blue), and −7.32 (blue) μC/cm^2 (a) for overall in the system, referenced to the potential of GR on the TOMAC4C4N side, and (b) in the vicinity of the TOMAC4C4N/EAN interface, referenced to the bulk potential of the TOMAC4C4N.

View Article Online
DOI: 10.1039/D6CP01551D

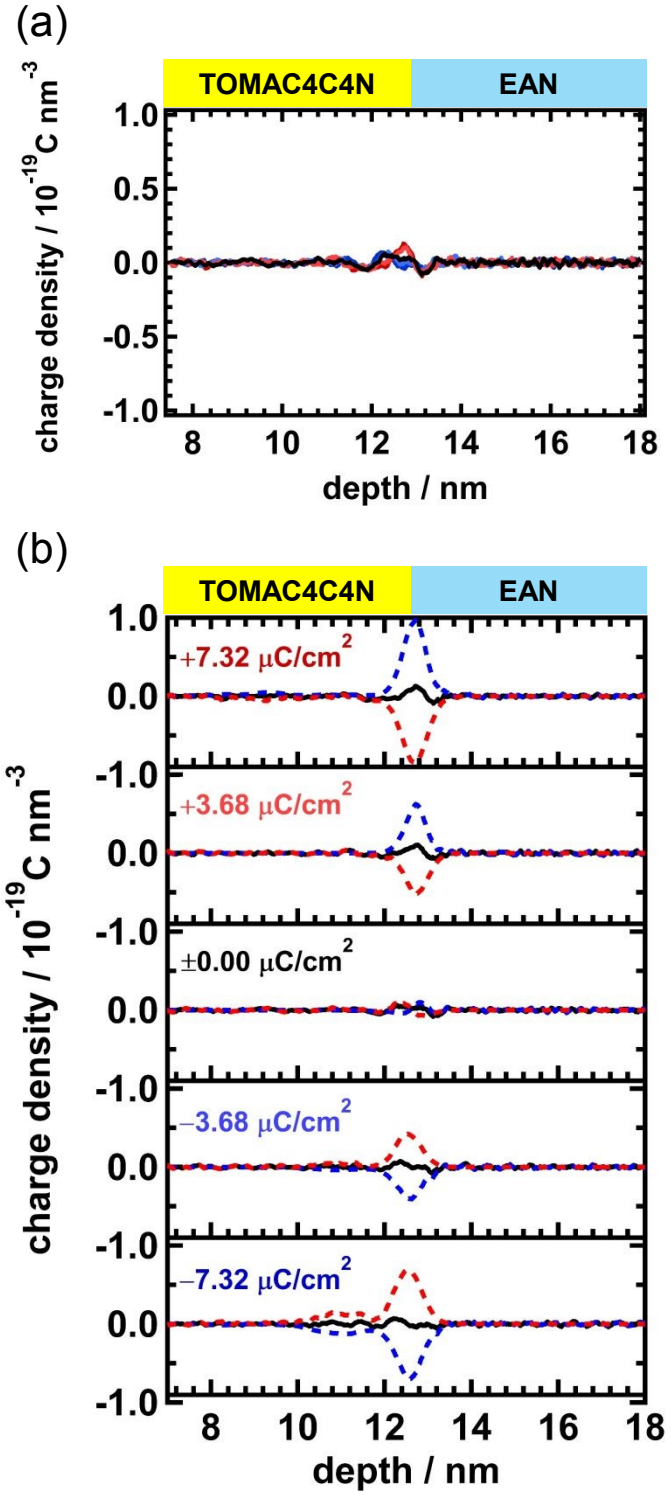

Fig. 5 Charge density distributions along the *z*-axis for (a) all ions in the system (black solid) at various $q_{\mathrm{GR,EAN}}$ values; +7.32 (dark red), +3.68 (red), 0.00 (black), −3.68 (light blue), and −7.32 (blue) μC/cm^2. and (b) all ions, and ions in the TOMAC4C4N (red dashed) and EAN (blue dashed) phases at various $q_{\mathrm{GR,EAN}}$ values.

View Article Online
DOI: 10.1039/D6CP01551D

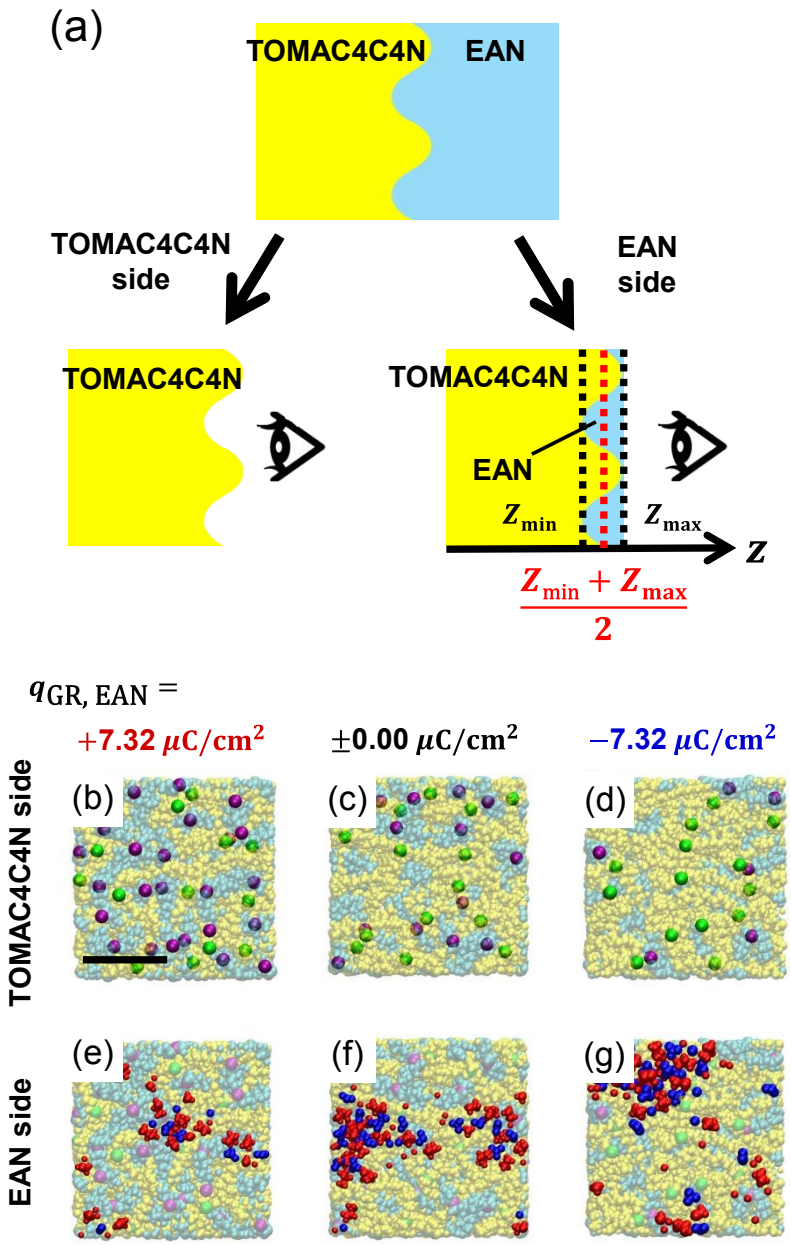

Fig. 6 (a) Two viewing ways of the interfacial structure at the TOMAC4C4N/EAN interface, where Z_{min} and Z_{max} are the minimum z-coordinate of the EAN atoms and maximum z-coordinate of the TOMAC4C4N atoms, respectively. (b-g) Snapshots of the interface at three $q_{\mathrm{GR,EAN}}$ values for the (b-d) TOMAC4C4N and (e-g) EAN sides. The color for each atom: (green) the N atom in $TOMA^+$, (yellow) the other atoms in $TOMA^+$, (purple) the N atom in $C4C4N^-$, (light blue) the other atoms in $C4C4N^-$, (red) EA^+, and (blue) NO_3^-. The scale is the same for all the snapshots (b-g) with the scale bar of 2 nm in (b).

View Article Online
DOI: 10.1039/D6CP01551D

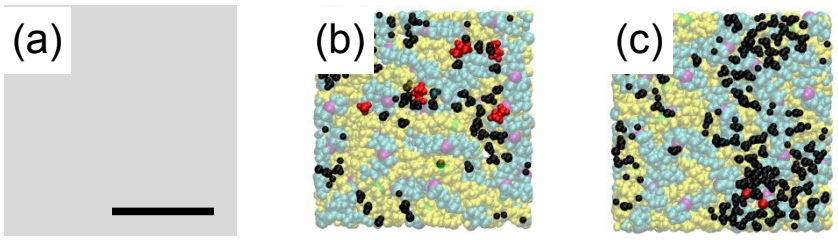

Fig. 7 Snapshots on the EAN side of the interface at +7.32 μC/cm^2 as in Fig. 6e at the (a) TOMAC4C4N/EAN, (b) TOMAC4C4N/W (EAN), and (c) TOMAC4C4N/W ($LiNO_3$) interfaces. The color definition is the same as in Fig. 6, with the addition of (black) water in Fig. 7b,c and (red) Li^+ in Fig. 7c. The scale is the same for all the snapshots (a-c) with the scale bar of 2 nm in (a).

View Article Online
DOI: 10.1039/D6CP01551D

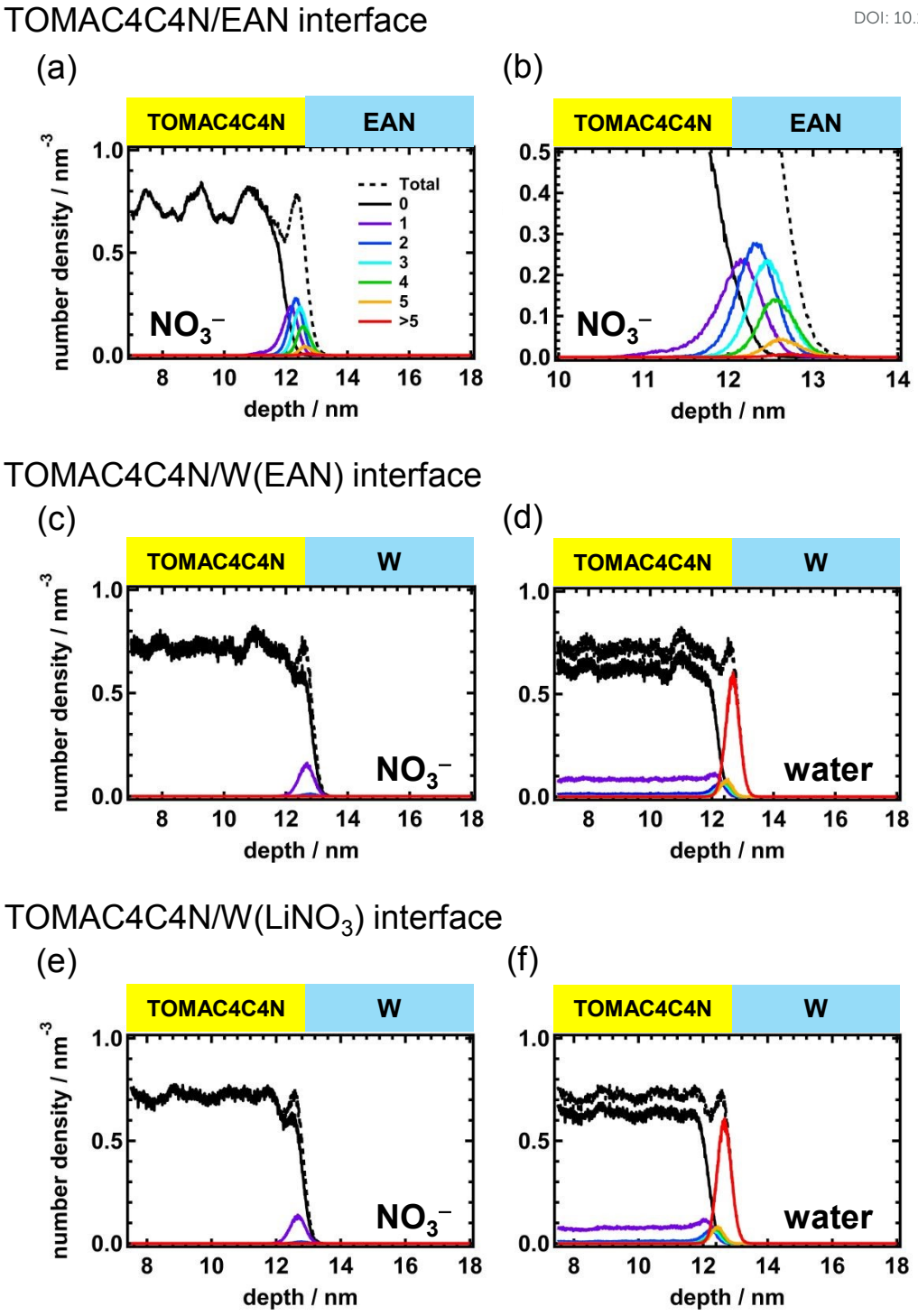

Fig. 8 Number density distribution of the N atom of $TOMA^+$ classified by the coordination number of the N atom of NO_3^- at the (a, b) TOMAC4C4N/EAN, (c) TOMAC4C4N/W(EAN), and (e) TOMAC4C4N/W ($LiNO_3$) interfaces and the O atom of water at the (d) TOMAC4C4N/W(EAN) and (f) TOMAC4C4N/W ($LiNO_3$) interfaces.

View Article Online
DOI: 10.1039/D6CP01551D

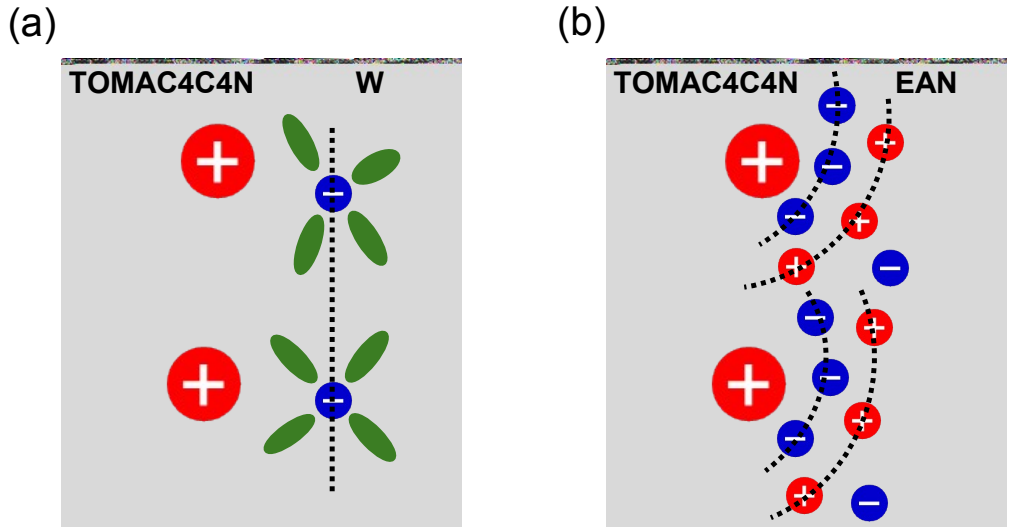

Fig. 9 Schematics of the structures of the (a) two-dimensional and (b) three-dimensional EDL at the liquid/liquid interfaces.

View Article Online
DOI: 10.1039/D6CP01551D

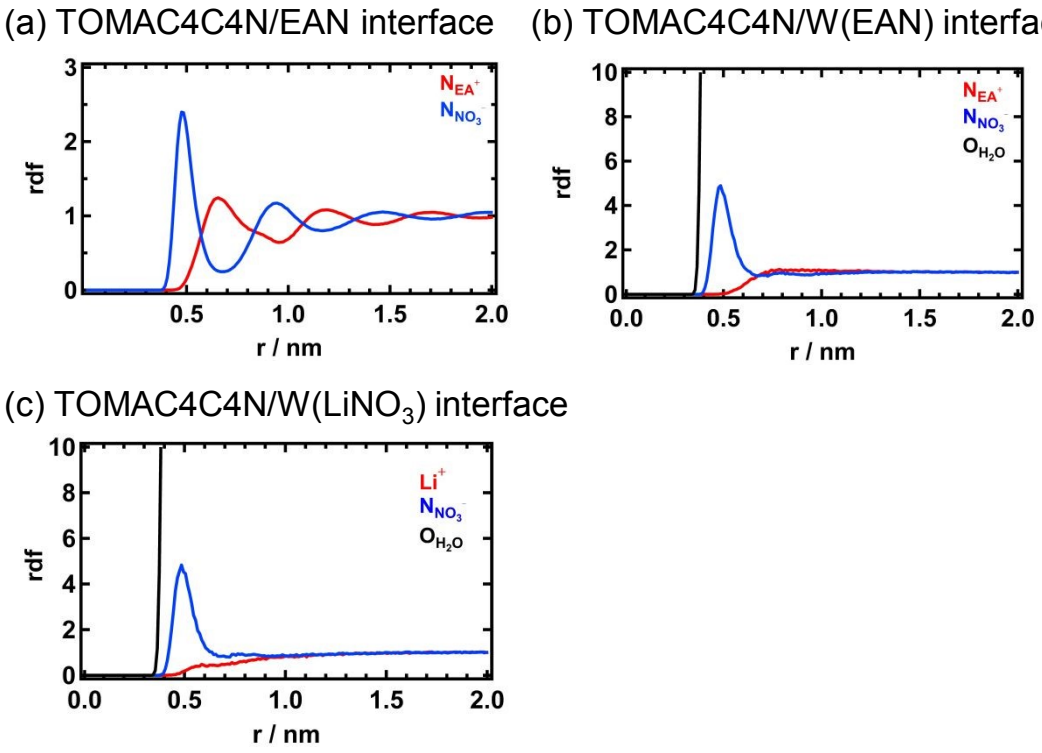

Fig. 10 Atom-atom RDF around the N atom of $TOMA^+$ at the (a) TOMAC4C4N/EAN, (b) TOMAC4C4N/W(EAN), and (c) TOMAC4C4N/W($LiNO_3$) interfaces at $q_{GR,EAN} = 0.00$ $\mu C/cm^{-2}$ for the N atoms of the (red) EA^+ or Li^+ and (blue) NO_3^-, and the O atom of (black) water.

View Article Online
DOI: 10.1039/D6CP01551D

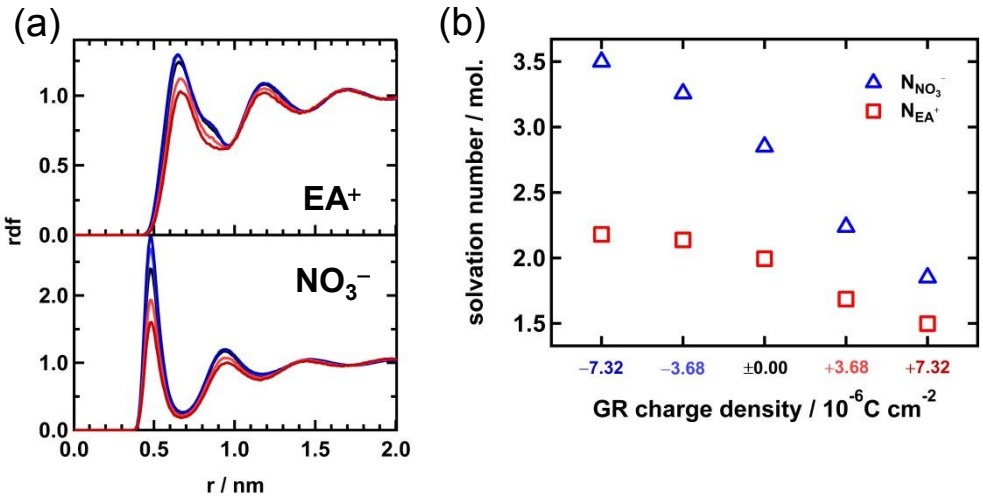

Fig. 11 (a) Atom-atom RDF around the N atom of $TOMA^+$ at the TOMAC4C4N/EAN interface coordinated with the N atom of (upper) EA^+ and (bottom) NO_3^- at various $q_{GR,EAN}$ values; +7.32 (dark red), +3.68 (red), 0.00 (black), −3.68 (light blue), and −7.32 (blue) $\mu C/cm^2$. (b) Coordination number at various $q_{GR,EAN}$ around the N atom of $TOMA^+$ at the TOMAC4C4N/EAN interface for the N atoms of (red) EA^+ and (blue) NO_3^-.

View Article Online
DOI: 10.1039/D6CP01551D

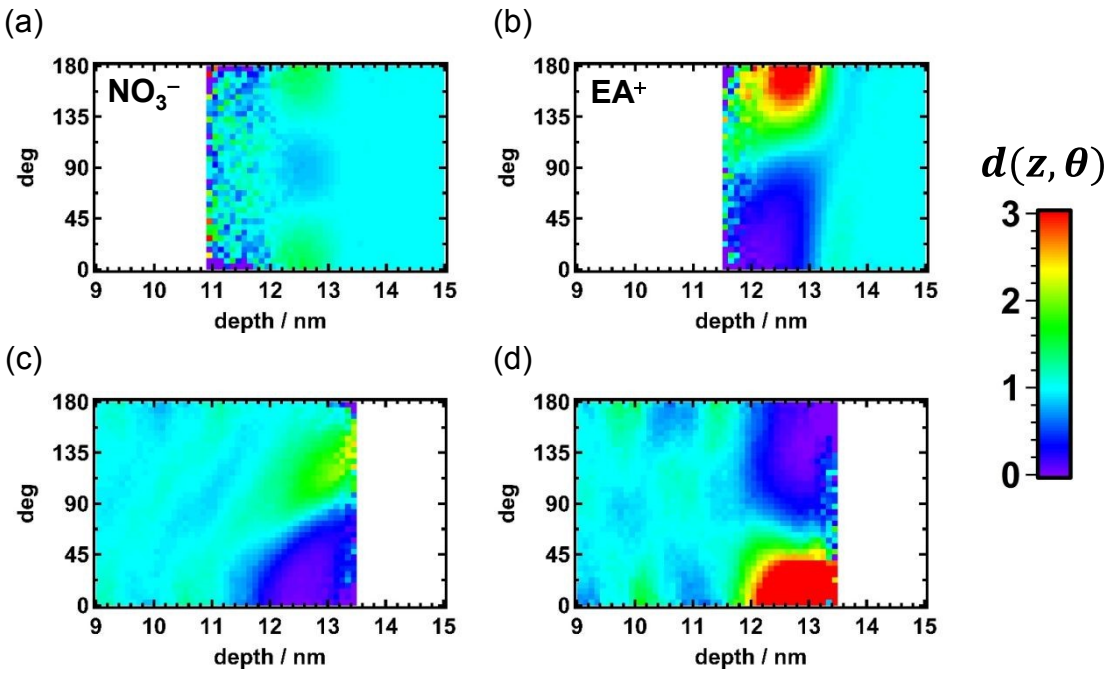

Fig. 12 Two-dimensional mapping of the orientational angle distribution along the *z*-axis for the (a) normal vector of three O atoms plane in NO_3^-, (b) N-C vector of EA^+, and (c) N-C_{octyl} and (d) N-C_{methyl} vectors of $TOMA^+$. The color scale of $d(z,\theta)$ represents the orientation distribution; $d(z,\theta) = 1$ is isotropic orientation, and $d(z,\theta) = 3$ is a polar orientation.

View Article Online
DOI: 10.1039/D6CP01551D

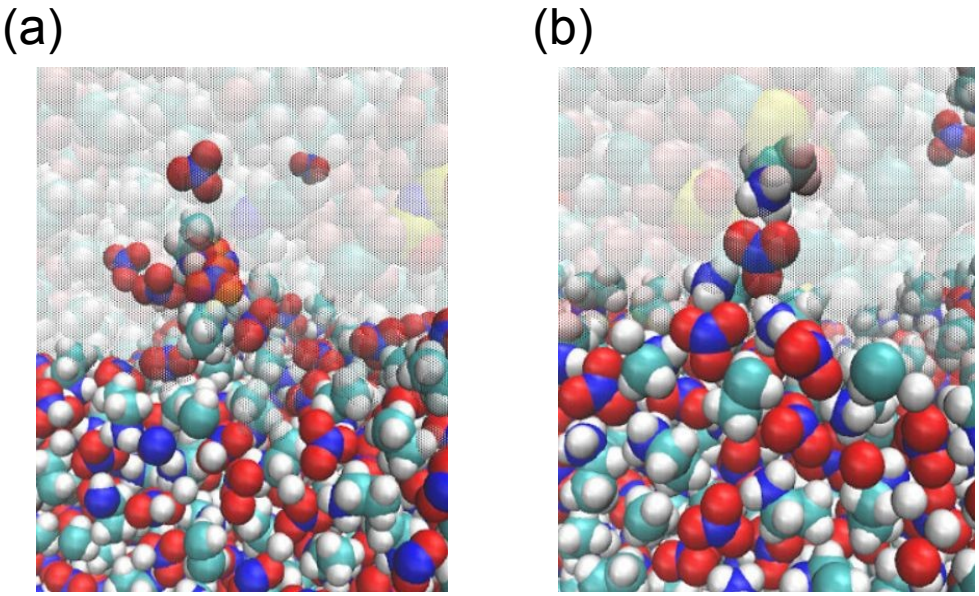

Fig. 13 Snapshots of ionic liquid fingers when (a) NO_3^- and (b) EA^+ are transferred from the EAN phase (lower) to the TOMAC4C4N phase (upper) across the IL/IL interface.

View Article Online
DOI: 10.1039/D6CP01551D

Data availability statement

The data supporting this article have been included as part of the Supplementary Information.